

TESTING THE POTENTIAL OF THE ITALIAN RADIO TELESCOPES FOR EUROPEAN RADAR OBSERVATIONS OF NEOs.

G. Pupillo⁽¹⁾, S. Righini⁽¹⁾, R. Orosei⁽¹⁾, C. Bortolotti⁽¹⁾, G. Maccaferri⁽¹⁾, M. Roma⁽¹⁾, M. Mastrogiuseppe⁽²⁾, T. Pisanu⁽³⁾, L. Schirru⁽³⁾, S. Cicalò⁽⁴⁾, A. Tripodo⁽⁴⁾, J. Harju⁽⁵⁾, A. Penttilä⁽⁵⁾, A. Virkki⁽⁵⁾, R. Ghiani⁽⁶⁾, M.N. Iacolina⁽⁷⁾, G. Valente⁽⁷⁾, D. Koschny⁽⁸⁾, and G. Sessler⁽⁸⁾

⁽¹⁾INAF-IRA, 40128 Bologna, Italy, Email: giuseppe.pupillo@inaf.it

⁽²⁾Sapienza Università di Roma - DIET, 00184 Roma, Italy

⁽³⁾INAF-OAC, 09047 Selargius, Italy

⁽⁴⁾SpaceDys s.r.l., 56023 Navacchio di Cascina, Italy

⁽⁵⁾University of Helsinki, 00014 Helsinki, Finland

⁽⁶⁾University of Cagliari, 09123 Cagliari, Italy

⁽⁷⁾Italian Space Agency, 00133 Roma, Italy

⁽⁸⁾ESA-ESOC, 64293 Darmstadt, Germany

ABSTRACT

In this work, we present preliminary results of NEO radar observations carried out by Italian radio telescopes in the framework of the ESA project “NEO observation concepts for radar systems”. It was aimed to derive the functional requirements of a radar system, evaluate the available European assets to perform NEO radar observations and carry out test radar campaigns. In the framework of this project, we performed observations of several asteroids, among which there were 2021AF8, 2016AJ193, and 4660 Nereus, which also served as test beds for the specific post-processing tools we developed. We also carried out the performance analysis of a possible European planetary radar system. Instrumental features, as much as issues like the impact of weather conditions on signal propagation at different radio frequencies, were considered. The European radio astronomical dishes, although employed only as receivers (in bistatic or multistatic configurations) and for a limited amount of time (due to their primary focus on other studies) might provide a significant contribution to the constitution of a European network for NEO monitoring and studies, if a transmitting antenna - equipped with a suitable high-power transmitter - were made available.

Keywords: Radar; NEO.

1. INTRODUCTION

Observations of NEOs are carried out by exploiting both optical and radar instruments. With respect to other techniques, radars allow observers to fully control the experiment parameters, as the transmitted signal is specifically tailored in terms of power, wavelength, polarization,

modulation, etc. The modifications observed in the reflected signal consequently provide accurate information about the dynamical and structural properties of the target. Radar observations are the method of choice to more accurately refine the target’s orbit and perform imaging (with a spatial resolution that can be of the order of a few metres). On the downside, being the strength of the radio echo inversely proportional to the fourth-power of the distance, radars are effective only at a relatively short distance or using high-power transmitters, which exist in a very limited number. Due to their restricted fields of view, radar systems cannot be used to survey the sky and detect new NEOs; they are instead employed to refine our knowledge of such new objects, even at a short distance from their discovery. The current NEO radar facilities transmit various waveforms with different parameters (e.g. bandwidth, modulation, etc.) depending on the specific experiment goals, target and system configuration (e.g. monostatic or bistatic). The different modes require specific post-processing and, in some cases, separate equipment. Often these different transmission modes alternate during the same observation campaign [6]. Quasi-monochromatic unmodulated continuous wave (CW) signals are used to determine some target characteristics such as radar cross-section, rotation rate and surface / near sub-surface information at wavelength scale. The CW waveform is also transmitted to measure the target Doppler shift with high precision for astrometric purposes. Delay measurements require modulated waveforms. Range-only measurements allow the refinement of the target ephemerides (as the Doppler-only measurements) and they are mainly used for astrometry purposes.

2. THE PROJECT

The European Space Agency issued a call for tenders (SSA P3-NEO-XXII, "NEO Observation Concepts for Radar Systems"), which has been successfully concluded, proposing a study on the requirements that a radar system must meet for NEO observations, both for scientific and planetary defense purposes, with specific attention to an evaluation of the European assets that might be employed/upgraded for such activities - also taking into account the tools and expertise that are needed in the post-observation phases. Test observations were an important part of this project, in view of the constitution of a possible future NEO European radar network led by ESA. The collaboration was conducted by SpaceDys and included INAF and the University of Helsinki, with the kind contribution granted by JPL for the execution of radar experiments.

2.1. Highlights from the study on general requirements and feasibility

The first part of the study was aimed at deriving the general functional requirements for a radar system dedicated to NEO observation for both astrometry and imaging. This general analysis covered many aspects, such as: Tx/Rx frequency, bandwidth, pointing and tracking accuracy, transmitted waveform (CW, amplitude, frequency and phase modulation, etc.), polarization, sensitivity, measurement resolution and accuracy. The following phase consisted in surveying the existing European facilities that might contribute to the constitution of a NEO radar system or network. The several medium-to-large diameter radio telescopes, though heavily scheduled with astrophysical activities, could be employed for a limited number of experiments, as receiving components in bistatic or multistatic observations. Moreover, Europe already hosts transmitting antennas (e.g. Cebros, TIRA, DSS63) whose potential, both considering the presently available transmitters and their possible upgrades, was analysed in our study.

To evaluate the performance of a NEO radar system, we considered different frequency bands, including not only the historically-employed ones, but also the possibility to operate at higher frequencies, in particular in Ka band (~ 34 GHz). We estimated the number of detectable NEOs per year - whose echo would exceed a given SNR value - as a function of the transmitted power, for four different transmitted frequencies: L (1.333 GHz), S (2.38 GHz), X (8.56 GHz) and Ka (34.0 GHz), corresponding to existing radar systems or taken into account for the possible design of future planetary radar instruments. The technical parameters were inspired by the ones characterizing real antennas, when such examples were available in the various bands, otherwise plausible values were desumed/rescaled according to literature. A standard atmospheric model [9] was applied to estimate the atmospheric attenuation and noise temperature at the considered frequencies in four weather scenarios. Such

weather profiles were derived from statistics measured at the Madrid DSN site [3]. As potential targets, we used the list of NEOs that had a close approach to Earth in the solar year 2020 at a distance ≤ 0.2 AU (divided in 3 size categories: all, ≥ 25 m, ≥ 140 m) and that were in the visibility window (target elevation $\geq 20^\circ$) of a radar located close to Madrid. An SNR cutoff value of ≥ 30 /track was adopted, as above this SNR threshold the rate of successful detection is close to 100% and accurate astrometry measurements can be performed [7]. A "readiness threshold" was also applied, in order to take into account a real-world scenario: targets with a discovery date closer than 5 days to their visibility window were discarded.

Figure (1) shows the expected yearly detections with $\text{SNR} \geq 30$ of asteroids larger than 25 m, if employing a 70-m antenna in monostatic mode under weather conditions defined as "average clear weather" ($\text{CD}=0.25$) and "very cloudy without rain" ($\text{CD}=0.90$). The CD value represents the statistics cumulative distribution of the described atmospheric conditions. For example, $\text{CD}=0.90$ means that 90% of the days (on a yearly basis) have atmospheric attenuation and noise temperature equal or better (i.e. lower) than the ones associated to the descriptive label. Figure (2) shows the results for a 35-m dish. It must be stressed that monostatic systems, though more easily manageable, reduce the observation efficiency by almost 50%, as transmission and reception take place alternatively. This means that, when longer integration times are needed, multistatic observations are more effective. These results clearly show how, given a certain transmitted power, a transmitter in Ka band is more productive than lower-frequency ones, even under a usually cloudy sky. Ka-band transmitters roughly need half the power required to reach a given performance in X band. Conversely, it must be noticed that, at such high power levels, X-band transmitters are presently the most used and better characterised, while Ka-band ones suffer from limitations - such as significant losses in the waveguides, not considered in our simulations. In comparison, the L band and S band choices - though weather-invariant - grant a much lower rate of successful observations, especially for dishes in the 35-m class, as their lower sensitivity further significantly reduces the number of possible detections.

2.2. Role and potential of the Italian facilities

The Italian National Institute for Astrophysics (INAF) manages three radio telescopes (Figure 3), located not far from the towns of Medicina, Noto and Cagliari. The latter is the Sardinia Radio Telescope (SRT), which is named Sardinia Deep Space Antenna (SDSA) when it works in its space configuration - as it is co-managed by ASI and is involved in deep space activities [10].

Table 1 summarises their main features. Details can be found in www.radiotelesopes.inaf.it

In the near future, all three Italian radio telescopes will be equipped with new tri-band K-Q-W receivers capable to acquire simultaneously the frequency bands 18-26,

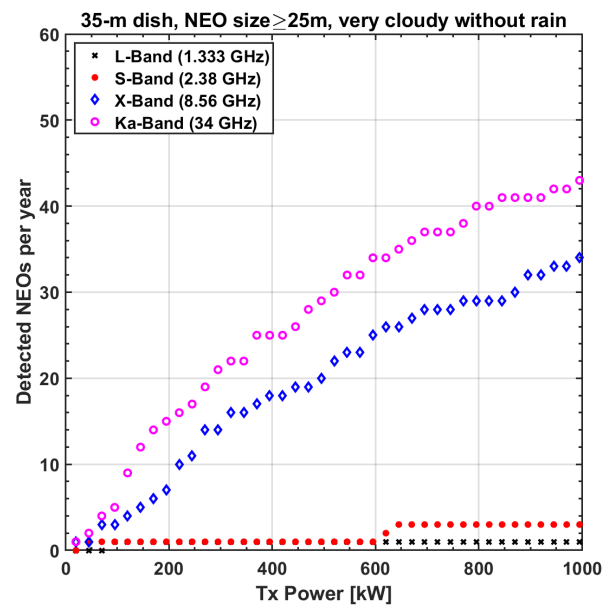
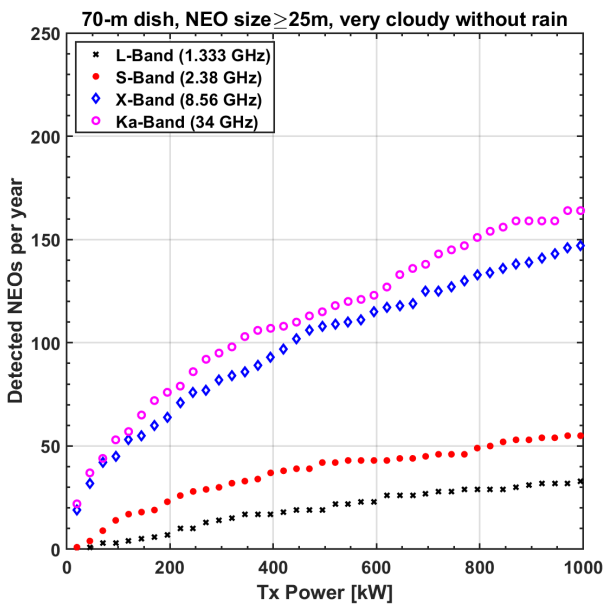
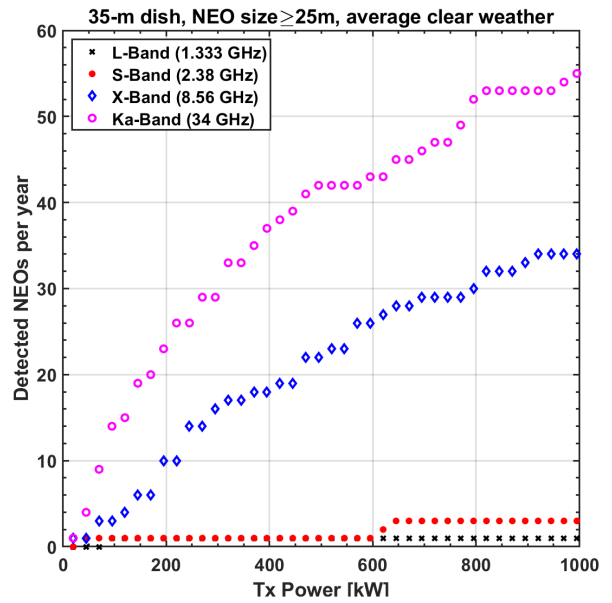
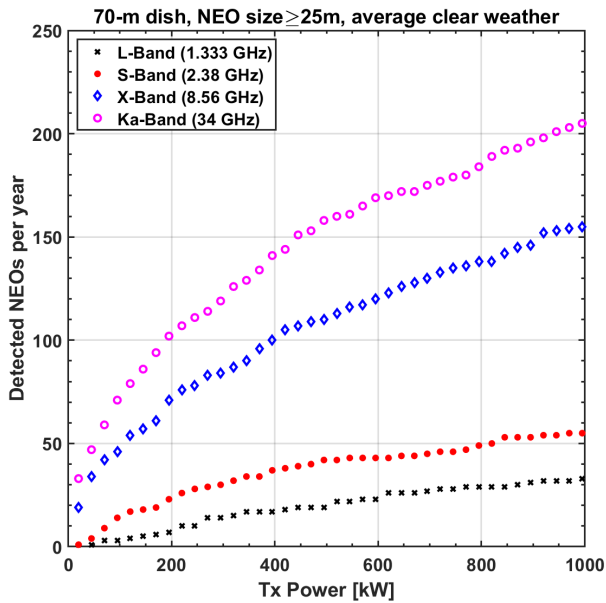


Figure 1. Number of expected yearly detections for a 70-m monostatic system as a function of frequency and power, considering different weather conditions.

Figure 2. Number of expected yearly detections for a 35-m monostatic system as a function of frequency and power, considering different weather conditions.



Figure 3. The three Italian radio telescopes. From left to right: SRT, Medicina dish, Noto dish.

Table 1. Main features of the Italian radio telescopes

	SRT/SDSA	Medicina	Noto
Diameter [m]	64	32	32
Rx (bands)	P,L,C,X,K	L,S,C,X,K	L,S,C,X,K
Active mirror	Yes	Imminent	Yes

33-50, 80-116 GHz. Moreover, the primary mirror of the Medicina dish is expected to be upgraded to an active surface in 2023, allowing to increase the antenna gain at higher frequencies and observe with flat gain at all elevations. SRT and the Noto dish are already provided with active mirrors.

3. THE EXPERIMENTS

In recent years, we carried out several NEO bistatic radar observations in which Italian radio telescopes were involved as receivers. In this section, as examples, we describe two of these experiments. For both, the transmitting antenna was DSS14 (Goldstone) in X-band planetary radar configuration. Further observations on other targets, involving as a transmitting station the DSS63 antenna (Madrid, equipped with a 20-kW 7.1-GHz transmitter), were also planned and successfully carried out in August and December 2022. Data is still under analysis and results will be discussed in forthcoming papers.

3.1. 2021AF8

Asteroid 2021AF8 was discovered in the framework of the Mt. Lemmon Survey, part of the Catalina Sky Survey (CSS) Program, on 2021 January 14. The object (see Table 2) is classified as a Potentially Hazardous Asteroid (PHA) by the International Astronomical Union's Minor Planet Center. Before radar observations, neither the size nor rotation period of this target was known. The size was estimated from its absolute magnitude, assuming a mean optical albedo of 0.14, as in the ESA Near-Earth Object Coordination Center (NEOCC) database (<https://neo.ssa.esa.int/>).

Table 2. Orbital and physical properties of asteroid 2021AF8, as they were known before radar observations

Designation	2021AF8
Epoch	59200.0 MJD
Orbit type	Apollo
Semi-major axis	2.01814 au
Eccentricity	0.515161
Inclination	9.698 deg
Long. ascending node	42.567 deg
Argument of perihelion	168.951 deg
Mean anomaly	315.866 deg
Orbital period	2.87 yr
Close approach distance	0.0224624 au
Close approach date	2021 May 04.50945
Absolute magnitude	(H) 20.2
Diameter	~300 m
Rotation period	unknown
Spectral class	unknown

Our radar observations devoted to 2021AF8 were carried out on 3 May 2021. They produced interesting results, thanks to the high sensitivity of the employed system, which involved DSS14 (Goldstone) for transmission and SRT/SDSA on the receiving side. Table 3 summarizes the main system parameters.

Table 3. System parameters for the observation of 2021AF8

	DSS14	SRT/SDSA
Type	Tx	Rx
Tx Frequency [MHz]	8560	-
Tx Power [kW]	450	-
Diameter [m]	70	64
Efficiency	0.64	0.54
System Temperature [K]	-	42
Polarization	RCP	LCP

Goldstone DSS14 scheduled radar observation of 2021AF8 in the monostatic configuration on May 3, 2021 from 15:05 UT to about 17:05 UT. JPL agreed to let us "eavesdrop" the echo signal during their monostatic observations and supply details on the transmission configuration timing (start/stop) and type. Since this DSS14 campaign was designed for a monostatic radar configuration:

- the frequency of the transmitted signal was modified in order to compensate for the Doppler variations - due to the known motion of the target (from ephemerides, dynamic compensation) - relative to the transmitting antenna DSS14 only. A signal re-

ceived at any other location would show a frequency drift;

- the observation needed to be divided into transmission/reception cycles (runs). Each run consisted of signal transmission for a duration close to round-trip light time (RTT) between the radar and the target, followed by a reception for a similar duration.

Both residual Doppler frequency drift and transmission On/Off runs are evident in the spectrogram of the received signal recorded at SRT/SDSA without Doppler compensation (Figure 4).

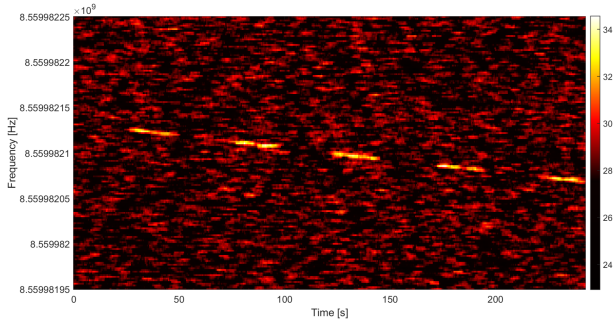


Figure 4. Spectrogram with 1.9 Hz/ch resolution, 5 s integration time, zoomed on the frequency interval around the echo. Color scale represents the power spectral density in dB-scaled arbitrary units.

The spectral smearing due to the frequency drift limits the maximum spectral resolution that can be achieved in the Doppler analysis and reduces the SNR. In order to remove the frequency drift, a Doppler compensation was thus performed by using a phase-stopping technique described in [4] and [5]. The frequency variation was modeled using a 3-rd order weighted least mean squares (WLMS) polynomial fit of the spectrum peaks exceeding a given SNR threshold (Figure 5).

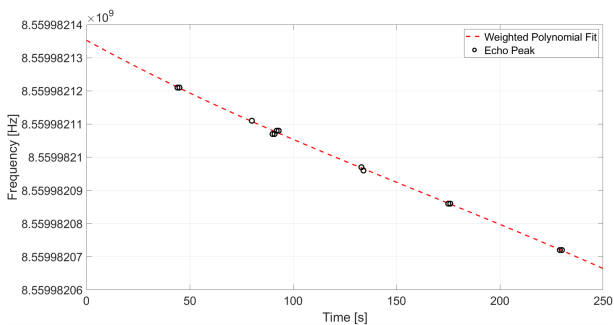


Figure 5. Peak detections with $SNR \geq 10$ (black circles) and the weighted polynomial fit of the frequency variations in time (dashed red line).

The successful removal of the frequency drift is evident in the spectrogram of the 2021AF8 signal (Figure 6) obtained from the time domain data after the Doppler compensation.

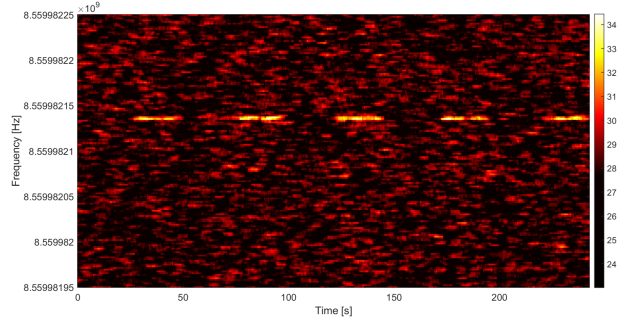


Figure 6. Spectrogram with 1.9 Hz/ch resolution, 5 s integration time, zoomed on the frequency interval around the echo, showing the Doppler-corrected data. Color scale represents the power spectral density in dB-scaled arbitrary units.

Data corrected for Doppler drift can produce high-resolution (sub-Hz) integrated power spectra (see Figure 7) because they are no longer affected by frequency smearing.

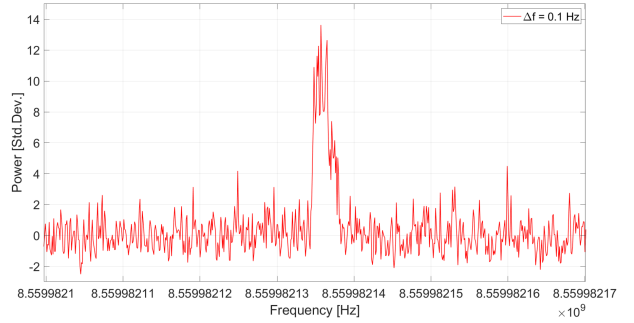


Figure 7. High-resolution integrated echo power spectrum of 2021AF8 (spectral resolution 0.1 Hz/ch)

The echo of the asteroid is well resolved in the high-resolution spectra. This allowed us to exploit the inverse of the formula of the echo Doppler broadening [8] (Equation 1) to estimate the asteroid rotation period :

$$B = \frac{4\pi D \cos(\alpha)}{\lambda P} \quad (1)$$

in which P is the target's rotation period, λ is the signal wavelength, B is the echo bandwidth and D is the projected diameter, and α and D are subradar latitude and the projected target's equatorial plane at the time of the observation, respectively.

Measurements of the Doppler broadening yielded an estimate of 2021AF8 rotation period ~ 8.5 hours, considering an equatorial view. The subradar latitude is unknown for a single measurement, therefore the value obtained is an upper limit of the effective target rotation period.

Since the SDSA receiver was capable to acquire only one polarization at a time, so it was not possible to estimate the polarization ratio in this experiment.

3.2. 4660 Nereus (1982DB)

Asteroid 4660 Nereus was discovered in February 1982 by E. F. Helin using the 18" Schmidt telescope at Palomar. Some of its physical properties were studied during the close approach in 2002. This object is elongated with an effective diameter of 330 meters, has a rotation period of 15 hours, and is a member of the optically-bright E spectral class. Nereus approached within 0.0263 au on December 11, 2021 and it was a strong radar target for several weeks.

Table 4. Orbital and physical properties of asteroid Nereus.

Designation	Nereus (1982DB)
Number	4660
Epoch	59600.0 MJD
Orbit type	Apollo
Semi-major axis	1.49 au
Eccentricity	0.359
Inclination	1.45 deg
Long. ascending node	313.15 deg
Argument of perihelion	159.54 deg
Mean anomaly	7.33 deg
Orbital period	1.81 yr
Close approach distance	0.026299 au
Close approach date	2021 December 11.57722
Absolute magnitude	(H) 18.3
Size	510 m x 330 m x 240 m
Rotation period	15.16 hrs
Radar albedo	0.44
Spectral class	Xe
Type	PHA, NHATS

During the period 10-15 December, Goldstone DSS14 scheduled observation of Nereus in Speckle interferometry mode, in which the VLBA (Very Long Baseline Array) was the receiving part. In agreement with L. Benner and M. Brozovic at JPL, Medicina joined the experiment in eavesdropping, in the following time intervals:

- 10 December, 2021 12:44:25 - 13:05:15 UT
- 15 December, 2021 12:20:00 - 12:40:00 UT

The main system parameters for the observation of Nereus with DSS14-Medicina are provided in Table 5.

In the radar Speckle experiments, similarly to a standard bistatic observation, CW transmission is employed without interruptions, but the Doppler is compensated for the Earth center - and not for a specific antenna. This leads to a residual Doppler shift in the received signal that we removed in post-processing through the phase-stopping method. Unlike the case of 2021AF8, here the phase polynomial coefficients were calculated from the ephemeris-based predictions provided by SpaceDys. Spectrograms of the Nereus echo in both polarizations,

Table 5. System parameters for the observation of 4660 Nereus

	DSS14	Medicina
Type	Tx	Rx
Tx Frequency [MHz]	8560	-
Tx Power [kW]	450	-
Diameter [m]	70	32
Efficiency	0.64	0.48
System Temperature [K]	-	38
Polarization	RCP	LCP, RCP

obtained from data (recorded on December 10th) with and without the Doppler compensation are shown in Figure 8 and 9, respectively.

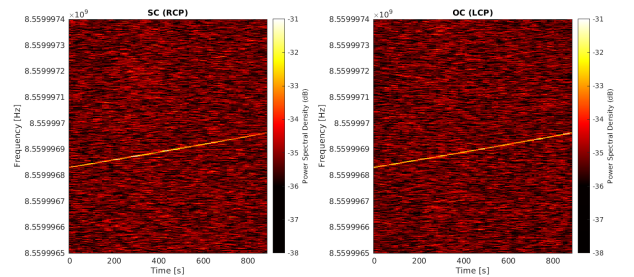


Figure 8. Spectrograms of Nereus echo in RCP (left panel) and LCP (right panel), without Doppler compensation. Color scale is the power spectral density in dB-scaled arbitrary units. Spectral resolution: 1Hz/ch, integration time: 30 s.

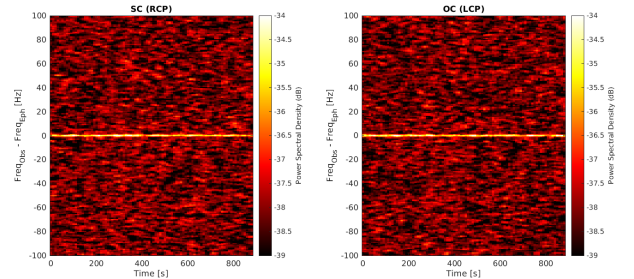


Figure 9. Spectrograms of Nereus echo in RCP (left panel) and LCP (right panel), from data after the Doppler compensation. Color scale is the power spectral density in dB-scaled arbitrary units. Spectral resolution: 1Hz/ch, integration time: 30 s.

High-resolution power spectra at 0.1 Hz/ch (see Figures 10 and 11) allowed us to measure both the frequency at the center of mass (COM) for astrometry computations and the asteroid rotation period. In the estimate of the echo broadening, besides the usual limb-to-limb Doppler bandwidth method, we employed also a multi-parametric fitting with a simple echo profile model [2].

In both days of observation, the measurements give a practically nil difference (within the measurement uncer-

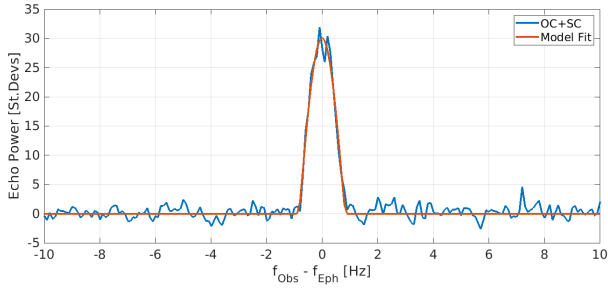


Figure 10. Integrated power spectrum at 0.1 Hz frequency resolution of the Nereus radar echo recorded at Medicina on December 10, 2021 (blue curve). Shape model fit (red curve).

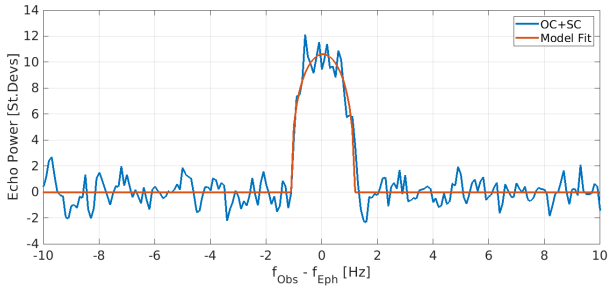


Figure 11. Integrated power spectrum at 0.1 Hz frequency resolution of the Nereus radar echo recorded at Medicina on December 15, 2021 (blue curve). Shape model fit (red curve).

tainties) between the observed COM frequency and that predicted by the ephemeris, testifying to the goodness of both the used ephemeris solutions and the Doppler compensation procedure in the time domain data. As concerns the echo bandwidth, measurements yielded: $B=1.7 \pm 0.1$ Hz for December 10 and $B=2.7 \pm 0.1$ Hz for December 15. The associated uncertainty is an inferior limit, referring to the spectral resolution only. To be conservative, a more realistic uncertainty of these echo bandwidth estimates could be around 0.5 Hz. Assuming Nereus's effective radius to be 330 m, and its rotation axis to be orthogonal to the line of sight (equatorial view), the already known 15.16 h rotation period would translate to an expected echo broadening of $B=2.2$ Hz for a signal at 8560 MHz frequency.

The discrepancy between the observed and expected echo bandwidth values, as much as the one between the two estimates obtained on different dates, might be due both to the elongated shape of the asteroid and to the actual subradar latitude angle (generally different from 0°) at the time of the observations.

In observations such as those of Nereus, in which the echo is detected in both polarizations, it is possible to calculate the circular-polarization ratio μ defined as:

$$\mu = SC/OC \quad (2)$$

where SC is the received echo power in the same polarization sense as transmitted and OC that in the opposite sense. The polarization ratio is one of the most important physical observables in the NEO radar technique, as it provides information about the asteroid surface and sub-surface roughness/complexity at the wavelength scale [11].

A preliminary analysis of our spectra indicates a high value of polarization ratio, typical of the E-class spectral type asteroids such as Nereus. This is in agreement with the measurements performed by Goldstone and Arecibo during the previous close approach [1]. More accurate evaluations will be possible once the optimisation of the analysis and de-Doppler procedures is complete.

4. CONCLUSIONS

The successful radar observations of various asteroids, carried out with the Italian radio telescopes, confirm the potential of these assets with respect to the opportunity of constituting a European network for NEO observations. Even if radio telescopes are heavily scheduled with other astrophysical programs, they can be involved in a select number of radar experiments, especially when high sensitivity and high efficiency are required. These instruments are already equipped with receivers in useful bands - even in high-frequency bands that have never been used for planetary radar up to now - and suitable back-ends. Furthermore, their staff already possess valuable know-how in radar observations and post-processing software development. Even though, at present, no suitable transmitting facility is available in Europe, there is significant interest in the constitution of a European network for NEO radar observations. The details necessary for its realization will likely be investigated in a near future.

ACKNOWLEDGMENTS

Observations were carried out within the ESA project "NEO Observation Concepts for Radar Systems" (SSA P3-NEO-XXII). These activities would not have been possible without the collaboration of JPL; we thank in particular Marina Brozovic and Lance Benner.

REFERENCES

1. Brozovic M., Ostro S.J., Benner L.A.M., Giorgini J.D., Jurgens R.F., Rosea R., Nolan M.C., Hineb A.A., Magri C., Scheeres D.J., Margot J.L. (2009). Radar observations and a physical model of Asteroid 4660 Nereus, a prime space mission target, *Icarus*, **201**, 153-166.
2. Jurgens R.F., Goldstein R.M., (1976). Radar observations at 3.5 and 12.6 cm Wavelength of Asteroid 433 Eros, *Icarus*, **28**, 1-15.

3. Kantak A.V., Slobin S.D., (2009). Atmosphere Attenuation and Noise Temperature Models at DSN Antenna Locations for 1–45 GHz, *JPL Technical Report*, **09-14**.
4. Molera Calvès G., (2012). Radio spectroscopy and space science with VLBI radio telescopes for Solar System research, *Ph.D. dissertation*, Aalto University, Pub. No. **42/2012**, [Online:] <http://lib.tkk.fi/Diss/2012/isbn9789526045818>.
5. Molera Calvès G., Pogrebenko S.V., Cimò G., Duev D.A., Bocanegra-Bahamòn T.M., Wagner J.F., Kallunki J., de Vincente P., Kronschnabl G., Haas R., Quick J., Maccaferri G., Colucci G., Wang W.H., Yang W.J., Hao L.F., (2014). Observations and analysis of phase scintillation of spacecraft signal on the interplanetary plasma, *A&A* **564**(A4), 1-7.
6. Naidu S.P., Margot J.L., Busch M.W., Taylor P.A., Nolan M.C., Brozovic M., Benner L.A.M., Giorgini J.D., Magri C., (2016). , Radar imaging and physical characterization of Near-Earth asteroid (162421) 2000 ET70, *Icarus*, **226**(1), 323-335.
7. Naidu S.P., Benner L.A.M., Margot J.L., Busch M.W., Taylor P.A., (2016). Capabilities of Earth-based radar facilities for near-Earth asteroid observations, *The Astronomical Journal*, **152**(4), 1-9.
8. Ostro S.J., (1993). Planetary radar astronomy, *Reviews of Modern Physics*, **65**(4), 1235-1279.
9. Shambayati S., (2008). Atmosphere Attenuation and Noise Temperature at Microwave Frequencies, *Low-Noise Systems in the Deep Space Network*, Chap. 6, JPL, Ed. by Macgregor S. Reid, Deep Space Communications and Navigation Series.
10. Valente G., Iacolina M.N., Ghiani R., Saba A., Serra G., Urru E., Montisci G., Mulas S., Asmar S.W., Pham T.T., de Vincente J., Viviano S., (2022). The Sardinia Space Communication Asset: Performance of the Sardinia Deep Space Antenna X-Band Downlink Capability, *IEEE Access*, **10**, 64525-64534.
11. Virkki A., Muinonen K., Penttilä A. (2014). Inferring asteroid surface properties from radar albedos and circular-polarization ratios, *Meteoritics & Planetary Science*, **49**(1), 86-94.